Nano-oxidation of silicon nitride films with an atomic force microscope: Chemical mapping, kinetics, and applications

F. S.-S. Chien, Y. C. Chou, T. T. Chen, W.-F. Hsieh, T.-S. Chao, and S. Gwo

Citation: Journal of Applied Physics **89**, 2465 (2001); doi: 10.1063/1.1339212
View online: http://dx.doi.org/10.1063/1.1339212
View Table of Contents: http://scitation.aip.org/content/aip/journal/jap/89/4?ver=pdfcov
Published by the AIP Publishing

Nano-oxidation of silicon nitride films with an atomic force microscope: Chemical mapping, kinetics, and applications

F. S.-S. Chien,[a] Y. C. Chou, and T. T. Chen
Department of Physics, National Tsing-Hua University, Hsinchu 300, Taiwan

W.-F. Hsieh
Institute of Electro-Optical Engineering, National Chiao-Tung University, Hsinchu 300, Taiwan

T.-S. Chao
National Nano Device Laboratory, 1001-1 Ta Hsueh Road, Hsinchu 300, Taiwan

S. Gwo[b]
Department of Physics, National Tsing-Hua University, Hsinchu 300, Taiwan

(Received 21 August 2000; accepted for publication 14 November 2000)

We demonstrate that local oxidation of silicon nitride films deposited on conductive substrates with a conductive-probe atomic force microscope (AFM) is a very promising approach for nanofabrication. Scanning Auger microscopy and spectroscopy are employed to verify the chemical changes after AFM-induced oxidation. Furthermore, the growth kinetics are found to have a logarithmic relationship of oxide height versus pulse duration $[h \propto \ln(t/t_0)]$. In contrast to rather slow thermal oxidation process, AFM-induced oxidation on silicon nitride has an anomalously high initial oxidation rate (~30 000 nm/s at 10 V) and a small onset time t_0 (~10 μs). As for the applications in ultrahigh-density recording, an oxide dot array (~100 Gbit/in.^{2}) produced by this process is demonstrated. The nitride film patterned by AFM can be utilized as an etching mask to fabricate ''subtractive'' silicon nanostructures, due to the large etching selectivity of $Si_3N_4:SiO_2:Si$ in various etchants. With this method, which is entirely compatible with the existing microelectronic processes, synthesis of ultrahigh packing density and ordered nanostructures could become readily achievable. © *2001 American Institute of Physics.* [DOI: 10.1063/1.1339212]

I. INTRODUCTION

Silicon nitride (Si_3N_4) is a dielectric material widely used for both silicon and gallium arsenide processing due to its many superior material properties. In contrast to SiO_2, Si_3N_4 has unique chemical, electrical, and mechanical properties. For example, it has larger dielectric constant (7.5 vs 3.9), refractive index (2.05 vs 1.46), and density (3.1 vs 2.2 g/cm^3), as compared with SiO_2.[1] In one of the most important applications, silicon nitride is used as an oxidation mask (oxidation rate is about 100 times less than silicon) during the local oxidation of silicon process.[2] In order to achieve high levels of integration and speed, the scaling of ultralarge-scale integrated (ULSI) circuits will develop into the nanometer regime (<100 nm) and ultrathin SiO_2 gate dielectrics of <2–3 nm thick will become necessary in the near future. To reduce the problem of direct tunneling in the case of ultrathin SiO_2, insulators with higher dielectric constants are more favorable as the gate dielectrics. Therefore, Si_3N_4 and silicon oxynitride (SiO_xN_y) thin films are particularly interesting for this application.[3] In addition, they have been used for passivation layers, barrier layers against impurity diffusion, ion implant masks, gate dielectrics in dynamic random access memory, and charge-trapping media in nonvolatile memory. The chemical selective etchings of oxide and silicon over nitride in many wet etchants[4,5] or dry processes[6] are also very important for the mask applications. As the decreasing of critical dimensions of ULSI circuits continues, an effective and reliable patterning process for silicon nitride film on the nanometer scale becomes increasingly significant.

Many researches have demonstrated that scanning probe microscope (SPM) induced oxidation can be used to achieve nanometer-scale patterning on semiconductors,[7–9] metals,[10–12] and to fabricate various devices, e.g., metal–oxide–semiconductor field effect transistor (MOSFET),[13] side-gated FET,[14] room-temperature single electron transistor,[15] and high-aspect-ratio and high-packing-density silicon nanostructures.[16] Recently, García *et al.*[17] reported the fabrication of high-areal-density oxide dot arrays on a hydrogen-passivated silicon substrate using noncontact atomic force microscopy (AFM) and Cooper *et al.*[18] reported the case of oxide array with an areal density of 1.6 Tbit/in.^{2} on a titanium film using a single-wall carbon nanotube grown on an AFM cantilever, revealing a new approach for ultrahigh-density data recording using AFM-induced oxidation. In principle, AFM-induced oxidation is a feasible process for nanometer-scale patterning on thin dielectric films deposited on conductive substrates. However, there are few reports in the literature to address this subject. In 1996, Day and Allee[19] reported the possibility of local oxidation on silicon nitride using the tungsten tip of a scanning tunneling

[a]Also with: Center for Measurement Standards, Hsinchu 300, Taiwan; Institute of Electro-Optical Engineering, National Chiao-Tung University, Hsinchu 300, Taiwan.
[b]Author to whom correspondence should be addressed; electronic mail: gwo@phys.nthu.edu.tw

microscope (STM). Very recently, we have successfully proved the conversion of Si_3N_4 to SiO_x with a conductive-probe AFM.[20]

In this article, we present the chemical analysis of the AFM-induced oxide using scanning Auger microscopy/spectroscopy (SAM/S) to show that AFM-induced oxidation is an effective method for conversion of silicon nitrides to oxides. We also present the oxide growth behavior and kinetics, although the exact AFM oxidation mechanism of silicon nitride is still unclear at this moment. Due to the small oxide onset time, the initial growth rate of oxide on silicon nitride is two orders of magnitude higher than that on silicon. Besides, we present examples of ultrahigh-density oxide dot array and nanostructures fabricated using a Si_3N_4 mask to demonstrate the prospective applications of AFM-induced oxidation on silicon nitride films.

II. EXPERIMENTAL CONDITIONS

The silicon nitride films were grown on *p*-type, 10 Ω cm, (100)-oriented Si wafers in a low pressure chemical vapor deposition (LPCVD) reactor at 780 °C using a mixture of $SiCl_2H_2$ (30 sccm) and NH_3 (130 sccm). Two films with thickness of 2.5 nm (sample A) and 5 nm (sample B) as measured by ellipsometry were used for this study. The sample B was further densified by rapid thermal anneal at 1000 °C in a nitrogen gas for 10 s. The film thickness was reduced to 4.2 nm after annealing. Local field-induced oxidation was performed with a commercial AFM/STM microscope operated in both contact and tapping modes in ambient air. The AFM cantilevers used for oxidation were highly doped (0.01–0.025 Ω cm) n^+-Si cantilevers. The typical tip radius, force constant, and resonance frequency of the contact mode cantilevers were 10 nm, 0.2 N/m, and 13 kHz, respectively. After coated with a 23 nm thick double layer of Cr and Pt/Ir, the typical tip radius became ~30 nm. The typical tip radius, force constant, and resonance frequency of the tapping mode cantilevers used were 10 nm, 32 N/m, and 273 kHz, respectively.

III. RESULTS AND DISCUSSIONS

A. SAM/S analysis

To investigate the conversion of silicon nitride to oxide, SAM/S was utilized to analyze the chemical composition. Three ~4×4 μm^2 squares on sample A were modified by the coated contact-mode cantilever at 0.4 μ m/s scan speed with a 10 V bias applied to the sample. Figure 1(a) is the scanning electron microscope (SEM) image, which shows the layout of the squares. The SAM mappings of the nitrogen and oxygen compositions at the same AFM-oxidized region are shown in Figs. 1(b) and 1(c), respectively, in which the gray level is proportional to the amount of the specific element. Obviously, in the modified area, the nitrogen content is suppressed but the oxygen content is enhanced. Auger spectra taken from the as-grown and modified areas are shown in Fig. 2. Both spectra have emission peaks of Si *LVV* at ~86 eV, Si *KLL* at ~1620 eV, and O *KLL* at ~512 eV. However, the peak of N *KLL* at ~385 eV in the as-grown area completely disappears after the film has been modified. Meanwhile, the magnitude of O *KLL* is much enhanced in the modified area as compared with that in the as-grown area. Therefore, it is clear that the nitrogen content is thoroughly replaced by the oxygen atoms. The results of SAM/S support the previous suggestion[12] that the nitride films can be converted to oxides by a SPM oxidation process. The mobile oxyanions (OH^-) drift toward the anodic substrate in response to the intense local field beneath the AFM tip and react with silicon nitride at the oxide/nitride interface while the nitrogen-related species drift outward.

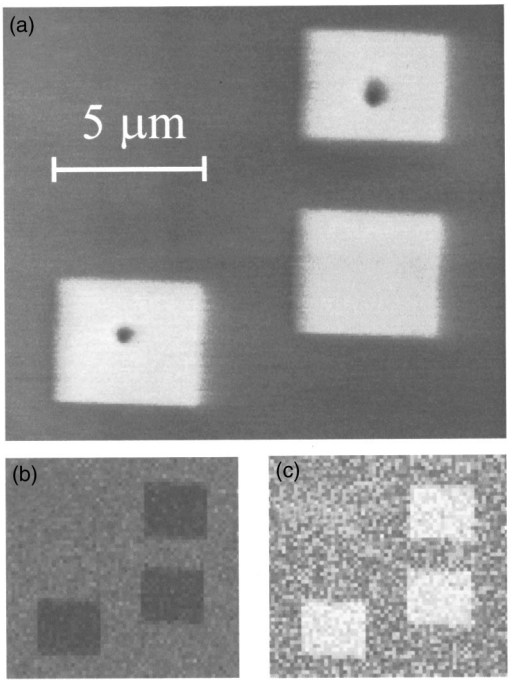

FIG. 1. (a) SEM micrograph of the AFM-induced oxide squares on the LPCVD Si_3N_4 film. Two black spots observed on the oxide patterns result from the electron-beam damaging during Auger analysis. (b) and (c) SAM mappings of the nitrogen and oxygen elements on the same region. The gray scale is used to represent the element contents (brighter regions contain more of the specified element).

In addition to the LPCVD films, we also applied the AFM-induced oxidation process on a single-crystal nitride film. The film was grown on a Si(111) substrate by thermal nitridation using ammonia. The Si(111)-(7×7) surface was prepared in an ultrahigh vacuum (UHV) chamber at a base

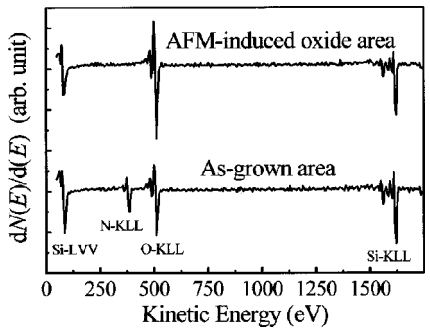

FIG. 2. Auger electron spectra at the AFM-induced oxide and as-grown areas of the LPCVD Si_3N_4 film.

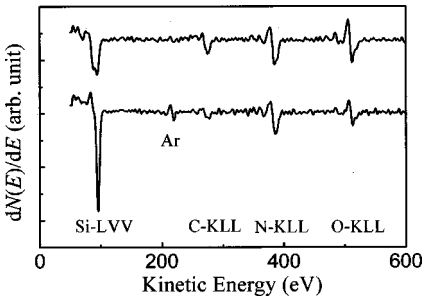

FIG. 3. Auger electron spectra taken on the single-crystal Si_3N_4 film before (upper spectrum) and after Ar ion sputtering (lower spectrum).

pressure of $<1\times10^{-10}$ Torr and heated to 900 °C for 20 min while NH_3 gas was leaked into the chamber at a pressure of 10^{-8} Torr (~12 L). The film thickness was estimated to be 2–3 nm according to previous reports.[21] The film was verified *in situ* by a UHV STM to be a single-crystal film with an (8×8) surface reconstruction.[22] Figure 3 is the Auger spectra of the films before and after Ar ion sputtering. Before sputtering, observations of the peak of N *KLL* at ~385 eV and the double peaks of Si *LVV* at ~88 (Si–N) and ~94 (Si–Si) eV are the evidence for silicon nitridation. The observed double Si-*LVV* peaks originate from the Si–N and Si–Si bonding, respectively. The peak of C *KLL* at ~267 eV indicates carbon contamination on the air-exposed surface. Argon ion sputtering of 3 keV accelerating voltage and 300 nA ion current was employed for 5 s to eliminate contamination. The sputtering rate of the film is about ~1–2 Å/s, therefore, corresponding to total sputtered film thickness of ~1 nm. The nitrogen content remains almost constant after sputtering, indicating the original nitride thickness was larger than 1 nm. On the other hand, the contents of oxygen and carbon were significantly reduced. The peak of elemental Si *LVV* at ~94 eV was much enhanced because the nitride film became thinner and the underlying Si substrate signal became more significant. AFM-induced oxides can also be produced on this type of film. Figures 4(a) and 4(b) are the AFM image and cross-section profile of AFM-induced oxide lines, and Fig. 4(c) is the AFM image of a 4×4 μm^2 oxide square produced by AFM on the film. The monolayer-height (~0.3 nm) steps in the modified square can be clearly observed even after AFM-induced oxidation, demonstrating that the AFM-induced oxidation process has an atomic smooth nature.

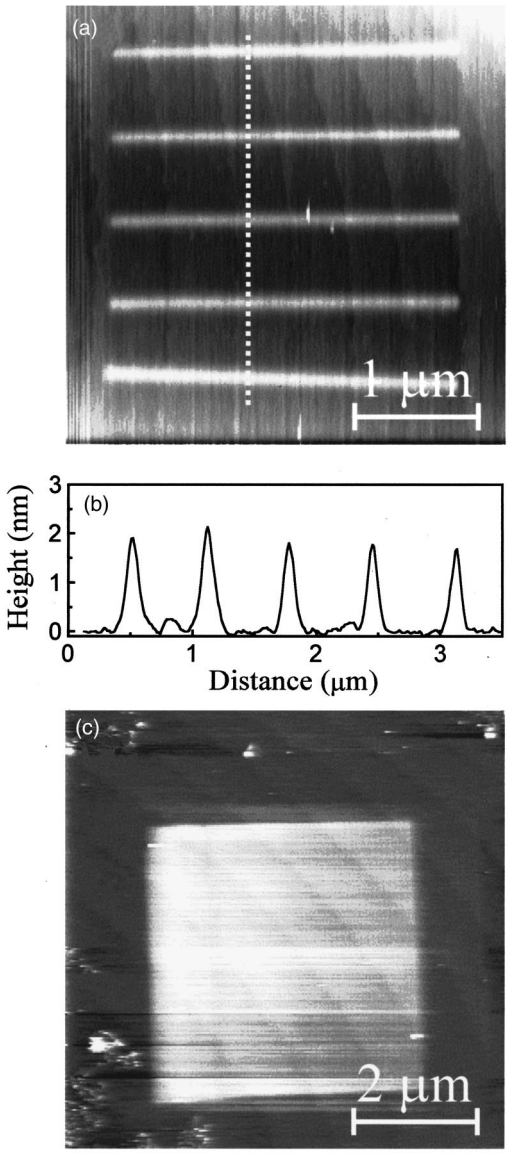

FIG. 4. AFM images of the AFM-induced oxide on the single-crystal Si_3N_4 film. (a) Oxide lines produced with 8 V bias, 0.06 μm/s writing speed. The oxide height is ~2 nm and the full width is ~250 nm. (b) Cross-sectional height profile along the marked line in (a). (c) 4×4 μm^2 oxide square produced with 10 V bias and 0.32 μm/s writing speed. The oxide height is ~4.4 nm.

B. Oxide growth kinetics

A clear understanding of the kinetics of AFM-induced oxidation is necessary to precisely control the oxide features. In the previous studies, Teuschler *et al.*[23] reported the empirical power law for the growth kinetics in which the height (h) is proportional to the γ power of pulse duration [$h(t)\propto t^{\gamma}$] with $\gamma = 1/4$ for the hydrogen-terminated Si(111). Based on the Cabrera–Mott theory[24] of field-induced ionic transport, Stiévenard *et al.*[25] found that the oxide growth kinetics can be described by the inverse-logarithmic form, where $1/h(t)=A-B\cdot\ln(t)$ (A and B are fit parameters). Avouris *et al.*[26] proposed the logarithmic kinetics in which the oxide height is proportional to the direct logarithm of pulse duration [$h\propto\ln(t)$] based on the data obtained by contact mode AFM oxidation on Si(100) substrates. An exponential dependence of oxidation rate on oxide height, $dh/dt\propto\exp(-h/L_c)$, can be deduced from this kinetics, where L_c is the characteristic decay length. They suggested that due to the fact that the molecular volume of SiO_2 is twice as large as that of Si, the development of stress leads to an additional activation energy barrier, causing rapid decrease of oxidation rate with increasing oxide height. Later, Calleja and García[27] observed the same logarithmic behavior by noncontact mode AFM oxidation on Si(100).

In 1956, Uhlig[28] obtained the direct-logarithmic form [$h(t)=k_0\cdot\ln(t/\tau+1)$] of oxide growth by assuming the oxidation rate is limited by the space charges increasingly trapped at and around the film–oxide interface. By using

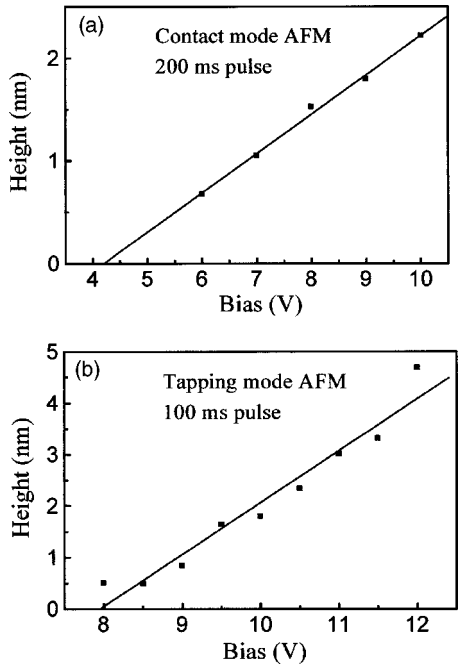

FIG. 5. (a) Plot of oxide height (h) vs applied bias (V) using a contact mode AFM with 200 ms pulse duration (the set point was 1 nN and feedback servo on) on the LPCVD Si_3N_4 film. (b) Plot of oxide height vs applied bias using a tapping mode AFM with 100 ms pulse duration (the feedback servo off during AFM oxidation) on the LPCVD Si_3N_4 film.

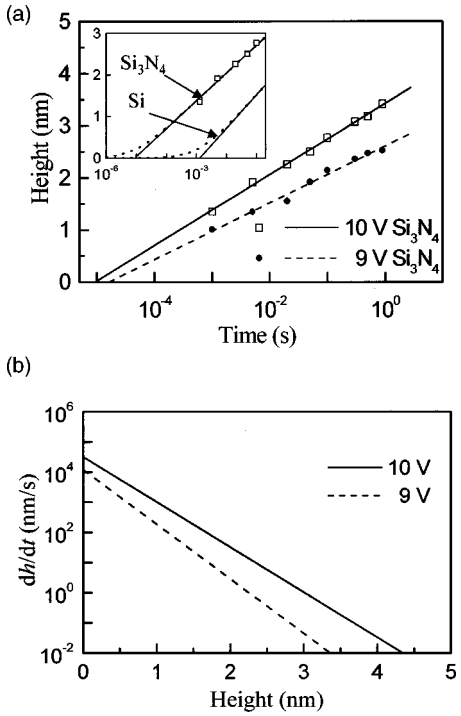

FIG. 6. (a) Oxide height plotted as a function of pulse duration (1 ms–1 s) on a logarithmic time scale at 9 and 10 V. The sample is the LPCVD grown Si_3N_4 film. The data points represent the experimental results averaged over several dots. In the inset, both types of logarithmic fittings [the dashed lines are fitted with $h(t)=k_0\cdot\ln(t/\tau+1)$ and the solid lines are fitted with $h(t)=L_c\cdot\ln(t/t_0)$] are displayed for comparison as well as the previously reported result on Si(100) (Ref. 27). (b) Exponential decay relation of the oxidation rate vs the grown oxide thickness [$dh/dt=R_0\cdot\exp(-h/L_c)$] derived from the kinetic data shown in (a), where R_0 is the initial oxidation rate and L_c is the characteristic decay length.

scanning Maxwell-stress microscopy, Dagata *et al.*[29] directly observed the trapped charge within the grown oxide. Recognizing that space charge buildup is the main rate-limiting step, Dagata *et al.*[30] further implemented the Uhlig model by explicitly incorporating the direct and indirect oxidation processes using the Alberty–Miller formalism[31] for AFM-induced oxidation on silicon. They discovered that AFM oxidation on Si exhibits a two-stage kinetics. In the transient region (~0.5 s for Si), both power law and Uhlig direct-logarithmic law are adequate in describing the oxidation behavior. However, after entering the steady-state growth region, a full consideration using the Alberty–Miller formalism is required. Recently, using the concept of space charge limited growth, Dubois and Bubendorff[32] have also successfully derived the power law form of AFM-induced anodic oxidation. For this work, we are interested in the initial growth rates of AFM-induced oxide on Si_3N_4 . Therefore, only the transient-region data are presented here and we use the direct-logarithmic formalism to fit our results. However, a full understanding of the oxidation kinetics may require data taken with longer oxidation time and a larger voltage range.

We studied the variation of oxide height with the applied voltage and exposure time on sample B using both contact and tapping modes of AFM. The AFM-induced oxide is topographically protruded since the molar volume of silicon oxide is larger than that of silicon nitride. Figure 5(a) and 5(b) are plots of the oxide height (h) versus applied voltage (V) for 200 ms pulse duration in contact mode and 100 ms in tapping mode, respectively. A linear dependence of oxide height on bias voltage with $h\propto V-V_{\rm th}$ is found, where $V_{\rm th}$ is the threshold voltage corresponding to ~4.3 and ~8 V for contact and tapping mode, respectively. The effective electrical field in the tapping mode is smaller for the dynamically oscillating cantilever and higher threshold voltage is required as compared with that of the contact mode.

For studying the oxidation kinetics, voltage pulses of various durations (1–1000 ms) were applied to the silicon nitride film and the patterned oxide dots were analyzed by contact mode AFM. Figure 6(a) displays the linear-log plots of oxide height versus pulse duration at biases of 9 and 10 V. The oxide height is found to increase as the logarithm of the pulse duration in both cases, that is similar to the empirical relationships obtained for silicon.[26,27] Instead of the Uhlig direct-log form, $h(t)=k_0\cdot\ln(t/\tau+1)$, where k_0 and τ are constants and $h(0)=0$, we find that it is better to fit the data with $h(t)=L_c\cdot\ln(t/t_0)$, where L_c is a voltage-dependent constant. By extrapolating the fitted straight line as $h(t)=L_c\cdot\ln(t/t_0)$ to the logarithmic time axis [as shown in Fig. 6(a)], we can find the oxide onset time t_0, which represents the period of time required for oxide to start growth upon applying voltage pulses. Also, an exponential decay relationship of the growth rate to oxide height $[dh/dt=R_0\cdot\exp(-h/L_c)]$ can be found from the kinetic data [Fig. 6(b)], where $R_0=L_c/t_0$ corresponds to the initial oxidation rate. Although the detailed chemical reactions are rather different, the AFM-induced oxidation process on both silicon nitride and silicon obeys the same logarithmic relationship of h and t and the expo-

TABLE I. Growth kinetic parameters of AFM-induced oxidation on silicon nitride and silicon.

	Bias (V)	L_c (nm)	t_0[a] (s)	R_0[b] (nm/s)
Si_3N_4 Contact mode	10	0.29	8.7×10^{-6}	3.3×10^{4}
	9	0.24	1.9×10^{-5}	1.3×10^{4}
Si[c] (Ref. 26)	10	0.39	4×10^{-2}	9.8
Si[d] (Ref. 27)	10	0.35	1.3×10^{-3}	250

[a]Determined by the intercept at the logarithmic t axis of the fitted line.
[b]Derived from L_c/t_0.
[c]By contact mode AFM, L_c is 0.9 nm$\times\log_{10}(e)$.
[d]By noncontact mode AFM, L_c is $0.1+0.03\times10-0.0005\times10^2$ (nm) and $t_0=\exp(-b/L_c)$, where $b=-2.1+0.5\times10-0.006\times10^2$ (nm).

nential decay relationship of dh/dt and h. The logarithmic relationship appears as a universal behavior of AFM-induced oxidation for most of materials studied in the transient region.

Table I shows the comparison of the oxide growth parameters (L_c, t_0, and R_0) of silicon nitride and silicon performed at similar sample biases. For silicon nitride, L_c is a linear function of bias voltage, consistent with the relationship of oxide height and bias at a fixed oxidation time ($h \propto V-V_{th}$). A proportional constant of characteristic decay length to bias is determined as $L_c/(V-V_{th}) = 0.051$ nm/V. Contrary to the thermal oxidation process[33] where the oxidation rate of silicon nitride is two orders of magnitude less than that of silicon, the silicon nitride film has much higher R_0 ($\sim$30 000 nm/s) compared with that of Si(100) (10–250 nm/s, Refs. 26 and 27) under similar experimental conditions. Since the magnitudes of L_c of silicon nitride and Si(100) at 10 V are about the same order of magnitude (0.29–0.39 nm), we conclude that the high initial oxidation rate of silicon nitride might result from the small oxide onset time ($\sim$10 μs), which is two orders of magnitude smaller than that of Si(100) ($\sim$1 ms) [see inset of Fig. 6(a)].

In our experiments, the electric field is weaker than in the case of a bare Si sample biased at the same voltage due to the starting thickness of the insulating nitride layer. The initial field intensity underneath the tip apex, calculated from the formula of Konsek *et al.*[34] for 30 nm tip radius, 10 V bias, and 4 nm separation between tip and Si substrate gap filled with Si_3N_4 (refractive index = 2) is about 1.2×10^9 V/m which is close to the critical field intensity for AFM-induced oxidation on Si(100).[26,35,36] On the other hand, the stress in silicon nitride films grown on silicon substrates is known to be tensile ($\sim1\times10^9$ dyn/cm^2), while the stress in silicon oxide films grown on silicon substrates is compressive ($\sim3\times10^9$ dyn/cm^2).[6] Therefore, the mismatch between SiO_x and Si_3N_4 is larger than that between SiO_x and Si. As a result, the AFM-induced oxide grown on silicon nitride contains more stress than that in the AFM-induced oxide grown on silicon substrates. Because of weaker electric field and larger compressive stress in the AFM-induced SiO_x, both thickness-limited[24] and stress-limited[26] kinetic models cannot account for the anomalously high oxidation rate observed on Si_3N_4. In addition, compared with the rate coefficient $A \cong 1$ nm/min$^{2/3}$ ($h=At^{2/3}$) for the wet thermal oxidation at 1100 °C and under 0.95 atm of water vapor,[37] and the rate of 0.82 nm/min for traditional anodic oxidation[38] with a field intensity of 1.9×10^9 V/m at 7.5 mA/cm^2, AFM-induced oxidation rate of Si_3N_4 is many orders of magnitude faster than the conventional methods.

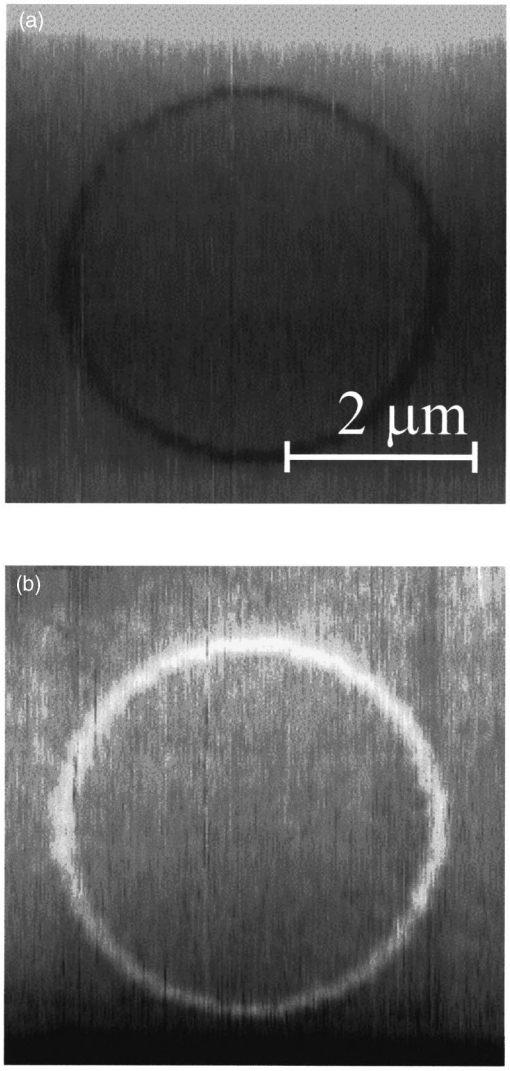

FIG. 7. (a) and (b) Contrast-reversed AFM images of an AFM-induced oxide circle on the LPCVD Si_3N_4 film taken with interleaved dual-scan mode (bottom-to-top and top-to-bottom scanning direction, respectively).

C. Image reversal

During our experiments, we sometimes observed the contrast reversal of contact-mode images of AFM-induced oxide taken interleavely with opposite-direction scans either bottom to top followed by top to bottom or left to right followed by right to left after the silicon cantilevers (metal coated or uncoated) had been used extensively. In Figs. 7(a) and 7(b), a 4.5 μm diameter oxide circle was produced by 10 V pulses and imaged with interleaved scans. A protruded topography of 1.5 nm height was recorded from the bottom-to-top scan, while a depressed one of 1.0 nm depth was obtained from the top-to-bottom scan. Occasionally, the ''apparent'' height or depth can be as large as 100 nm. Definitely, the real AFM-induced oxide height cannot be so

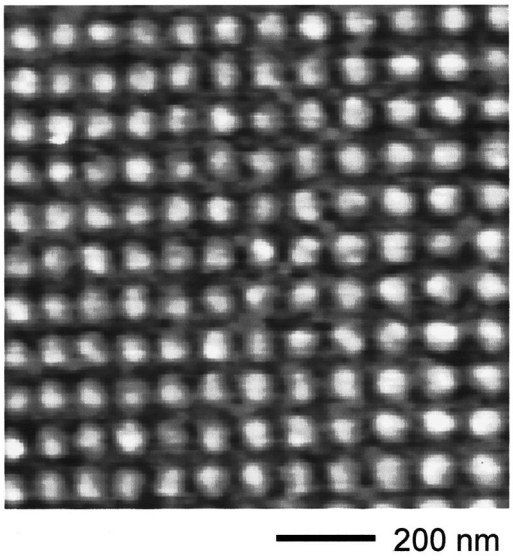

FIG. 8. Oxide dot array of 100 Gbits/in.^{2} bit areal density on the LPCVD Si_3N_4 film. This dot array is obtained by applying pulses of +9 V and 5 ms duration on the predetermined locations with a tip moving speed of 0.5 μm/s. The total writing time is ~30 s for this array.

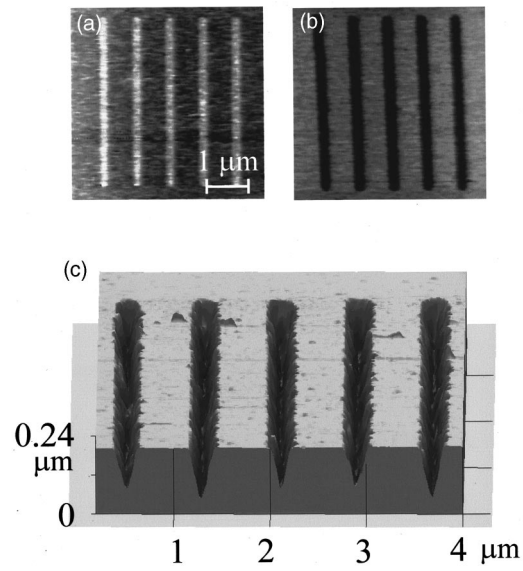

FIG. 9. (a) AFM image of oxide lines on the LPCVD Si_3N_4 film. (b) Trenches on the same region after dipping in HF solution. (c) AFM image of the *V*-grooved Si structure on the same region after KOH etching.

large. Such a topographic reversal phenomenon was also observed for the AFM-induced oxide on silicon substrates. We believe that the space charges trapped in the grown oxide cause the image reversal. Space charges exert additional forces on the worn cantilevers and cause the response of the optical-lever feedback system[39] to maintain a constant bending of the cantilever. Throughout our oxidation experiments discussed above for kinetics study, we always took AFM images in both scan directions to make sure that nearly identical oxide topographic heights were obtained, excluding factitious effects from the trapped space charges.

IV. APPLICATIONS FOR DATA RECORDING AND NANOSTRUCTURE FABRICATION

Two of the most prospective applications of AFM-induced oxidation are ultrahigh-density data recording and AFM nanolithography process. In this section, we will present examples of AFM-induced oxidation on silicon nitride films for high-density surface modification and nanostructure fabrication. Shown in Fig. 8, we generated an oxide dot array with an areal density of ~100 Gbit/in.^{2} on sample B by applying pulses of +9 V and 5 ms duration on the predetermined locations with a tip moving speed of 0.5 μm/s. The total writing time is ~30 s for this array. The oxide formation is very reproducible and uniform with ~45 nm dot diameter and ~1.2 nm oxide height. The AFM-induced oxidation on nitride film can be used as a write-once and read-many data recording technique with a higher areal density than the predicted superparamagnetic limit for the magnetic recording. Compared with hydrogen-passivated silicon substrates and titanium films oxidized in ambient, silicon nitride film is more superior as a data recording medium due to its resistance to oxidation under ambient conditions. Additionally, the high initial oxidation rate of silicon nitride requires a shorter writing time, so higher recording speed can be achieved. It should be noted that the slow probe speed (0.5 μm/s) used here is only due to the instrumentation limit. With the current advances in high-speed,[40] large-area,[41] and parallel-probe[42,43] methods, the fundamental limit to the writing speed using this approach is the initial oxidation rate.

The patterned nitride films can be used as etch masks due to the large etch selectivity of silicon nitride to oxide and silicon. The etching rates in 1% HF solution determined by ellipsometry are 0.01 nm/s for the sample B and 0.27 nm/s for AFM-induced oxide, corresponding to an etch selectivity of 27. Therefore, HF dipping can remove the AFM-induced oxide without substantial etching to the nitride film. The patterned windows, exposing the Si substrate, can be used for subsequent fabrication process development of nanostructures.

The etching rate of silicon nitride film in a KOH solution is very slow. Under some conditions,[4] the selectivity of Si/Si_3N_4 in a KOH solution is extremely high (1000:1). For the usage of the AFM oxidation technique, a thin mask film is preferred to produce high-areal-density patterned Si-exposing windows. Hence, before patterning, the nitride film (sample B) was thinned to 3 nm thick (measured by ellipsometry) by dipping in a 1% HF solution for 120 s. Figure 9 shows the process to produce a *V*-groove Si structure. First, oxide lines parallel to the ⟨110⟩ direction were written with 10 V bias and 0.08 μm/s writing speed [Fig. 9(a)]. The oxide is 2 nm high and with a full width at half maximum (FWHM) of 210 nm. After the sample was dipped in a 1% HF solution for 20 s at 26 °C, the oxide lines were selectively removed and the topography converted to 3 nm deep trenches with a FWHM of 230 nm [Fig. 9(b)]. The conversion ratio of total oxide volume to the consumed silicon volume defined by total oxide height divided by the buried oxide depth is about 1.67. After subsequent etching in a 20

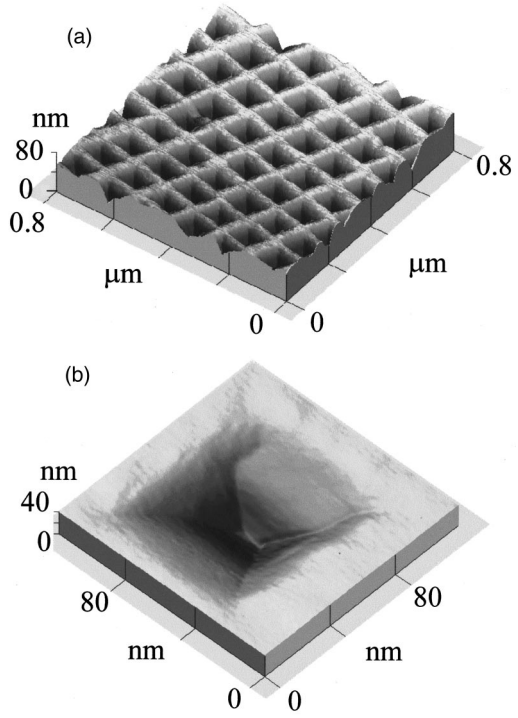

FIG. 10. (a) AFM image of an array of inverted pyramid pits on the Si substrate. (b) Perspective view of a single inverted pyramid pit.

wt % KOH solution for 20 s at 50 °C to transfer the pattern into silicon substrate, the *V*-groove terminal geometry is formed by two intersecting {111} crystal planes because of the anisotropic etching of silicon in KOH [Fig. 9(c)]. The *V*-groove opening on the surface is about 350 nm and depth is 150 nm.

Figures 10(a) shows an example of inverted pyramid pit array in Si. First, an oxide dot array pattern was made by applying +9 V pulses of 5 ms duration. The produced oxide dots have an average diameter of ~60 nm and a protruded oxide height of ~2 nm. After pattern transfer using aqueous KOH, each oxide dot converts to a $\sim 60 \times 60$ nm^2 pit [Fig. 10(b)]. The inverted pyramidal etching pits, independent of the mask opening shape, are formed with four intersecting {111}-crystal-planes. And the etched depth is self-limited by the terminal etch geometry. This ''subtractive'' process could be used for fabricating nanostructures from thin films or multilayered structures, or as high-density read-only memory. Additionally, the ''subtractive'' structures can be utilized as templates for selective growth since the deposited materials tend to grow over the unmasked silicon surfaces. Recently, single-crystal silicon dots and lines have been successfully grown by selective CVD with AFM-patterned Si_3N_4/SiO_2bilayer growth masks.[44]

V. CONCLUSIONS

SAM and SAS have been used to prove the conversion of LPCVD-grown Si_3N_4 to SiO_x by a conductive-probe AFM. The electrical field under the AFM tip promotes the bi-directional diffusions of O- and N-related species, although the exact reaction paths are still unknown. We also show that the AFM-induced oxidation performed on the single-crystal silicon nitride film is an atomic smooth process. In the study of oxidation kinetics, the oxide height is found to be linearly proportional to the bias applied to the sample in both contact and tapping modes of AFM. In addition, the oxide growth kinetics obeys the logarithmic relationship of oxide height and pulse duration as $h(t)=L_c \cdot \ln(t/t_0)$, which is similar to the previous results on Si(100) conducted by contact and noncontact modes. We find that the initial oxidation rate R_0 can be related to L_c/t_0. Due to its anomalously small oxide onset time t_0 (~10 μs), the initial growth rate (~30 000 nm/s at 10 V) of oxide on nitride films is two orders of magnitude higher than that on silicon substrates under similar conditions. It is surprising that AFM-induced oxidation on elementary materials (e.g., Si) and on compounds (e.g., Si_3N_4) has the same growth kinetics and Si_3N_4, traditionally used as an oxidation mask, has an extremely high initial oxidation rate. The role of nitrogen seems to be critical for this process. Further studies are necessary to reveal the exact cause of these phenomena.

For practical applications, we have demonstrated two examples to show the feasible applications of AFM oxidation of nitride films on the nanometer scale. First, the AFM oxidation of nitride films can be employed for ultrahigh-density (~100 Gbit/in.^{2}) data recording with the advantages of high writing speed and resistance to oxidation under ambient conditions. Second, with the large etching selectivity of silicon and oxide to nitride, the patterned nitride film can be employed as an etching mask to fabricate subtractive nanostructures (e.g., *V*-grooves and inverted pyramid pit array), which can be used as templates for selective-area growth (an ''additive'' process) or nanomechanical devices.

ACKNOWLEDGMENTS

The authors thank Dr. J. A. Dagata (NIST) for useful discussions on the AFM oxidation kinetics, J.-W. Chang and S.-W. Lin for technical assistance. This work was partly supported by the National Science Council (Contract Nos. NSC-89-2112-M-007-077 and NSC-89-2112-M-009-071) and the Program for Promoting Academic Excellence of Universities (Contract Nos. 89-FA04-AA and 89-E-FA06-I-4), the Ministry of Education, Taiwan.

[1] S. M. Sze, *Physics of Semiconductor Devices*, 2nd ed. (Wiley, New York, 1981), p. 852.
[2] S. A. Campbell, *The Science and Engineering of Microelectronic Fabrication* (Oxford University Press, New York, 1996), Chap. 15, p. 390.
[3] *Fundamental Aspects of Ultrathin Dielectrics on Si-Based Devices*, edited by E. Garfunkel, E. P. Gusev, and A Vul' (Kluwer, Dordrecht, 1998).
[4] Etch rate selectivity of $Si_3N_4:SiO_2:Si$ in diluted HF (40%) at room temperature is about 1:>100:0.1 and in aqueous KOH (30 wt %) at 60 °C 1:>14:> 2600; S. D. Collin, in *Semiconductor Micromachining*, edited by S. A. Campbell and H. J. Lewerenz (John Wiley & Sons, Chichester, 1998), Vol. 2, Chap. 2, p. 57 and p. 65.
[5] Etch rate selectivity of $Si_3N_4:SiO_2:Si$ in H_3PO_4 (94.5%) at 180 °C is about 10:<1:0.3; W. van Gelder and V. E. Hauser J. Electrochem. Soc. **114**, 869 (1967).
[6] M. Madou, *Fundamentals of Microfabrication* (CRC, Boca Raton, 1997), Chaps. 2 and 5.
[7] J. A. Dagata, J. Schneir, H. H. Harary, C. J. Evans, M. T. Postek, and J. Bennett, Appl. Phys. Lett. **56**, 2001 (1990).
[8] J. A. Dagata, W. Tseng, J. Bennett, C. J. Evans, J. Schneir, and H. H. Harary, Appl. Phys. Lett. **57**, 2437 (1990).

[9] E. S. Snow and P. M. Campbell, Appl. Phys. Lett. **64**, 1932 (1994).
[10] H. Sugimura, T. Uchida, N. Kitamura, and H. Masuhara, Jpn. J. Appl. Phys., **32**, L553 (1993).
[11] D. Wang, L. Tsau, K. L. Wang, and P. Chow, Appl. Phys. Lett. **67**, 1295 (1995).
[12] S. Gwo, C.-L. Yeh, P.-F. Chen, Y.-C. Chou, T. T. Chen, T.-S. Chao, S.-F. Hu, and T.-Y. Huang, Appl. Phys. Lett. **74**, 1090 (1999).
[13] S. C. Minne, H. T. Soh, Ph. Flueckiger, and C. F. Quate, Appl. Phys. Lett. **66**, 703 (1995).
[14] P. M. Campbell, E. S. Snow, and P. J. McMarr, Appl. Phys. Lett. **66**, 1388 (1995).
[15] K. Matsumoto, M. Ishii, K. Segawa, Y. Oka, B. J. Vartanian, and J. S. Harris, Appl. Phys. Lett. **68**, 34 (1996).
[16] F. S.-S. Chien, C.-L. Wu, Y.-C. Chou, T. T. Chen, S. Gwo, and W.-F. Hsieh, Appl. Phys. Lett. **75**, 2429 (1999).
[17] R. García, M. Calleja, and H. Rohrer, J. Appl. Phys. **86**, 1898 (1999).
[18] E. B. Cooper, S. R. Manalis, H. Fang, H. Dai, K. Matsumoto, S. C. Minne, T. Hunt, and C. F. Quate, Appl. Phys. Lett. **75**, 3566 (1999).
[19] H. C. Day and D. R. Allee, Nanotechnology **7**, 106 (1996).
[20] F. S.-S. Chien, J.-W. Chang, S.-W. Lin, Y.-C. Chou, T. T. Chen, S. Gwo, T.-S. Chao, and W.-F. Hsieh, Appl. Phys. Lett. **76**, 360 (2000).
[21] I. J. R. Baumvol, Surf. Sci. Rep. **36**, 1-166 (1999).
[22] S. Gwo, C.-L. Wu, F. S.-S. Chien, and T. Yasuda, Jpn. J. Appl. Phys. (submitted).
[23] T. Teuschler, K. Mahr, S. Miyazaki, M. Hundhausen, and L. Ley, Appl. Phys. Lett. **67**, 3144 (1995).
[24] N. Cabrera and N. F. Mott, Rep. Prog. Phys. **12**, 163 (1948–1949).
[25] D. Stiévenard, P. A. Fontaine, and E. Dubois, Appl. Phys. Lett. **70**, 3272 (1997).
[26] Ph. Avouris, T. Hertel, and R. Martel, Appl. Phys. Lett. **71**, 285 (1997).
[27] M. Calleja and R. García, Appl. Phys. Lett. **76**, 3427 (2000).
[28] H. H. Uhlig, Acta Metall. **4**, 541 (1956).
[29] J. A. Dagata, T. Inoue, J. Itoh, and H. Yokoyama, Appl. Phys. Lett. **73**, 271 (1998); J. A. Dagata, T. Inoue, J. Itoh, K. Matsumoto, and H. Yokoyama, J. Appl. Phys. **84**, 6891 (1998).
[30] J. A. Dagata, F. Perez-Murano, G. Abadal, K. Morimoto, T. Inoue, J. Itoh, and H. Yokoyama, Appl. Phys. Lett. **76**, 2710 (2000).
[31] R. A. Alberty and W. G. Miller, J. Chem. Phys. **26**, 1231 (1957).
[32] E. Dubois and J.-L. Bubendorff, J. Appl. Phys. **87**, 8148 (2000).
[33] A. E. T. Kuiper, M. F. C. Willemsen, J. M. L. Mulder, J. B. Oude Elferink, R. Erens, F. H. P. M. Habraken, and W. F. van der Weg, J. Vac. Sci Technol. B **7**, 455 (1989).
[34] S. L. Konsek, R. J. N. Coope, T. P. Pearsall, and T. Tiedje, Appl. Phys. Lett. **70**, 1846 (1997).
[35] F. Marchi, V. Bouchiat, H. Dallaporta, V. Safarov, D. Tonneau, and P. Doppelt, J. Vac. Sci. Technol. B **16**, 2952 (1998).
[36] P. A. Fontaine, E. Dubois, and D. Stiévenard, J. Appl. Phys. **84**, 1776 (1998).
[37] T. Enomoto, R. Ando, H. Morita, and H. Nakayama, Jpn. J. Appl. Phys. **17**, 1049 (1978).
[38] T. B. Tripp, J. Electrochem. Soc. **117**, 157 (1970).
[39] D. Sarid, *Scanning Force Microscopy*, 2nd ed. (Oxford University Press, New York, 1994), Chap. 10.
[40] S. C. Minne, G. Yaralioglu, S. R. Manalis, J. D. Adams, J. Zesch, A. Atalar, and C. F. Quate, Appl. Phys. Lett. **72**, 2340 (1998); S. C. Minne, S. R. Manalis, and C. F. Quate, *Bringing Scanning Probe Microscopy Up To Speed* (Kluwer, Boston, 1999).
[41] S. C. Minne, J. D. Adams, G. Yaralioglu, S. R. Manalis, A. Atalar, and C. F. Quate, Appl. Phys. Lett. **73**, 1742 (1998).
[42] P. Vettiger, J. Brugger, M. Despont, U. Drechsler, U. Dürig, W. Häberle, M. Lutwyche, H. Rothuizen, R. Stutz, R. Widmer, and G. Binnig, Microelectron. Eng. **46**, 11 (1999).
[43] G. Binnig, M. Despont, U. Drechsler, W. Häberle, M. Lutwyche, P. Vettiger, H. J. Mamin, B. W. Chui, and T. W. Kenny, Appl. Phys. Lett. **74**, 1329 (1999).
[44] T. Yasuda, S. Yamasaki, and S. Gwo, Appl. Phys. Lett. **77**, 3917 (2000); S. Gwo, T. Yasuda, and S. Yamasaki, J. Vac. Sci. Technol. A (to be published).